Mechanical dissolution of copper additions in aluminium by Friction Stir Processing

M. Gnedel, A. Zens, Ferdinand Haider, M. F. Zaeh

Angaben zur Veröffentlichung / Publication details:

Gnedel, M., A. Zens, Ferdinand Haider, and M. F. Zaeh. 2019. "Mechanical dissolution of copper additions in aluminium by Friction Stir Processing." *IOP Conference Series: Materials Science and Engineering* 480 (Conference 1): 012020. https://doi.org/10.1088/1757-899x/480/1/012020.

Mechanical dissolution of copper additions in aluminium by Friction Stir Processing

IOP Conf. Series: Materials Science and Engineering 480 (2019) 012020 doi:10.1088/1757-899X/480/1/012020

Mechanical dissolution of copper additions in aluminium by Friction Stir Processing

M Gnedel[1,*], A Zens[2], F Haider[1] and M F Zaeh[2]

[1] Chair for Experimental Physics I, University of Augsburg, Universitätsstraße 2, 86159 Augsburg (Germany)
[2] Institute for Machine Tools and Industrial Management, Technical University of Munich, Boltzmannstraße 15, 85748 Garching (Germany)

[*] e-mail: maximilian.gnedel@physik.uni-augsburg.de

Abstract. Friction Stir Processing (FSP) can be used to locally modify properties in materials such as aluminium. Furthermore, the composition of the alloy can be changed by this technique. Intermixing specific micrometer-sized metal powders as well as metal foils helps to optimize both the microstructural stability during subsequent heat treatment, as well as the mechanical properties in general. Dispersing copper powder inside a matrix of AA1050 aluminium by FSP can produce homogenous solid solution of the two elements, if suitable processing parameters are used. A substantial hardening effect is shown for both effects, refinement of the grain structure and solid solution hardening. By calculating the diffusion length and using the results of investigations based on energy-dispersive X-ray spectroscopy (EDS), it can be shown that the dissolution is mainly mechanically driven and not due to diffusion. Furthermore, transmission electron microscopy (TEM) provides insights on the formation of intermetallic phases during FSP. The results may be used in future studies to evaluate the properties of such non-equilibrium alloys.

1. Introduction

Local enhancement of materials properties in light metals through a change in the microstructure and chemical composition is a topic with extensive research focus within physical metallurgy these days. In most cases, this is accomplished with the assistance of a high degree of plastic deformation, which is widely referred to as mechanical alloying. A variety of techniques can be applied for this purpose and many different metallic systems have already studied in order to evaluate if plastic deformation can help to create advantageous metallic composites or even highly supersaturated solid solutions.

1.1. Conventional techniques for mechanical alloying

The first attempts at mechanical alloying were performed over 20 years ago by ball milling of metal powders with steel or ceramic spheres. At that time, the combination of copper and a variety of other elements was the primary focus [1–3]. However, this technique has continued to draw a large amount of attention and persists even today. A wide range of different material combinations have been tested and successfully brought to amorphisation, depending on the heat of mixing [4].

With high pressure torsion (HPT), extreme amounts of plastic deformation can be applied to metallic materials. As with ball milling, the focus of studies up to this point has been primarily copper-based systems, and depending on the composition of the base composition and on the relative strength of the

components, composites similar to solid solutions have been obtained even for immiscible combinations [5,6] in equilibrium.

Accumulative roll bonding is also widely used to produce solid mixtures of metals under high plastic deformation. Often, aluminium is used as base material and, for example, mechanically alloyed with nickel as a harder alloying partner. Similar to the high pressure torsion experiments, the relative mechanisms of deformation to fracture are studied [7]. The Al-Cu system has gained much attention for processing with this technique; thus, the results of the conducted experiments can serve as reference values for the experiments done by FSP [8,9].

1.2. FSP for mechanical alloying

It has been shown, that FSP is an effective technique for distributing additional alloying elements in various geometries like powder, wire or foil inside an aluminium matrix [10]. Especially for visualizing the material flow during the process, Cu foil pieces were used so far [11].
Mechanical alloying with powder is still the dominating method to integrate additional elements. Fe is for example a widely used alloying partner besides Cu [12][13].

Different goals are the driving forces for these studies, depending on the chosen element. Whereas in the Al-Fe system often the magnetic properties are studied, the addition of Zr can help to improve the microstructural stability [14]. Most elements are integrated to improve the mechanical properties like hardness or fracture toughness, which also holds for Cu [15–18]. Furthermore, the Al-Cu system, which is effectively hardenable by producing the Θ' phase (Al_2Cu) during annealing and together with the unique microstructure obtained by FSP is very promising for applications where high strength and light weight metal parts are needed. The local modification of structural parts by mechanical alloying with Cu is imaginable, but not yet studied.

Apart from the goal of producing an alloy with supreme mechanical properties, the mechanisms of intermixing during this process of partly diffusion, partly mechanical driven mixing have to be understood. Al-Cu as modelling system for soft/soft and partly miscible interaction is, besides the advantageous mechanical properties, an excellent system to examine this. It was already shown, that Cu powder can extensively be dissolved by FSP [19], but the crucial influencing variables are not yet identified.

2. Experimental and analytical set-up

2.1. Experimental set-up

Figure 1 shows a schematic diagram of the experimental set-up, in which two EN AW-1050 sheets are aligned in butt-joint configuration. Copper powder, inserted in a groove in the middle of the sheets, is distributed in the weld nugget during processing. The thickness of the sheets was 8.0 *mm* and the dimensions of the groove where 1 *mm* x 0.5 *mm* filled with commercially pure copper CW008A powder with an average particle size of 3-4 μm. The probe performed either 2 or 4 passes through the material, for which the rotation direction was kept constant. Hereby, the advancing and retreating sides changed for each pass. The tool dimensions were 12 *mm* for the shoulder diameter, 5.0 *mm* for the base and 3.6 *mm* for the tip diameter of the conical probe, and 3.5 *mm* for the probe length. The shoulder plunge depth was 0.1 *mm* and a tool tilt angle of 2 ° was employed. The probe was threaded and furnished with three uniformly distributed flats. A CNC milling machine (Heller MCH250), which has been adapted to perform FSW processes, was used in position-controlled mode for all experiments.

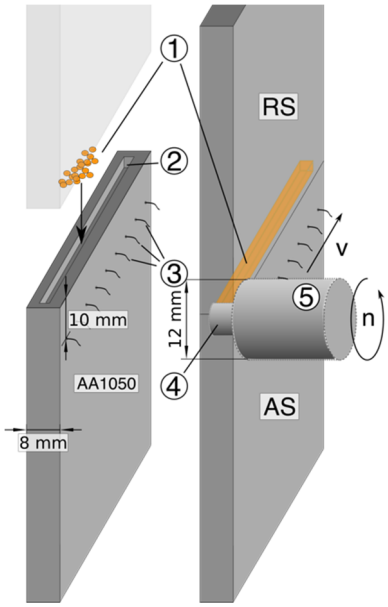

Figure 1. Schematic diagram of the sample production by a combination of Friction Stir Welding and Friction Stir Processing of the joint of two aluminium sheets with copper powder (1) in between. A groove (2) in the lower sheet is filled with commercially pure copper and the temperature during the process is measured by thermocouples (3). A rotating steel probe (4) with a shoulder (5) distributes the additional copper within the Aluminium matrix.

Nine Type K thermocouples with a size of 0.5 *mm* in diameter where placed inside holes 10 *mm* away from the joint. The holes were 0.6 *mm* in diameter and had a depth of 2 *mm*. The specimens for the hardness and compositional analysis where taken from the middle of the 286 *mm* long seam in order to ensure, that the analysis was preformed within an area in which the process was stable. The feed rate, rotation speed, and number of passes for each experiment can be found in Table 1.

Table 1. Process parameters for the production of the welding seams investigated in this work.

Sample	Feed rate (*mm/min*)	Rotation speed (*RPM*)	Number of passes
1	50	1500	2
2	50	2250	2
3	50	1500	4

2.2. Analytical set-up

One specimen was extracted for each seam at approximately 143 *mm* from the starting point of the weld for hardness measurements and electron microscopy. The cross sections were prepared metallographically for scanning electron microscopy (SEM) with a final chemomechanical polishing using 40 *nm* silica particles. The specimens for transmission electron microscopy (TEM) were electrolytically thinned. High resolution SEM was executed using a ZEISS MERLIN microscope. A JEOL JEM-2100F allowed TEM with a resolution up to atomic scale.

3. Results and discussion

3.1. Structure

The structural properties of the samples where investigated by light- and electron microscopy techniques, to study distribution, dissolved Cu fraction and possible precipitations formed during the process. An extensive study with the same experimental setup but coarser Cu powder and lower rotation rates preceded this study, but never led to particle dissolution.

Figure 2 shows a macrograph of a cross section of sample 2, which was polished, etched with Kroll's reagent and recorded with a light microscope. The cross section was also prepared at a second position approximately 2 *cm* further along the welding direction, which led to a nearly identical result. This shows, that the process is stable in the investigated region. Dissolved Cu is clearly visible as dark contrast, which is proven by energy dispersive X-ray (EDX) analysis (Figure 3-5). Few undissolved clusters can be identified as bright spots. The shape of the dissolved Cu resembles a marble cake, which already points to a complicated mechanical distribution during FSP. Sample 1 does not show any dissolution of Cu, whereas sample 2 and 3 both show rather homogenous distribution of dissolved Cu in the whole stir zone, which for sample 2 is remarkable, due to the execution of only two passes. A clearly defined border is visible at the bottom of the stir zone and the advancing side, which was investigated in detail, using electron microscopy.

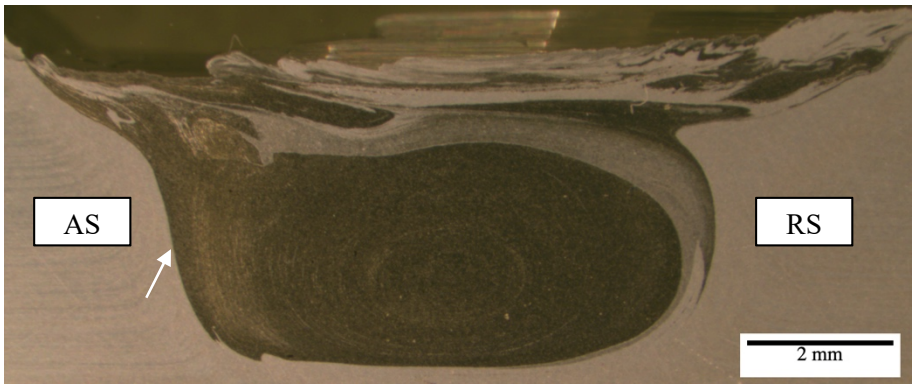

Figure 2. Macrograph of cross section of sample 2 taken with a light microscope after polishing and etching with Kroll's reagent. Advancing and retreating side of the second pass as well as the position of EDX analysis are marked.

In Figure 3 and 4 the edge region of sample 2 and 3 at the position marked in Figure 2 is shown, where Cu found by EDX analysis is displayed in red. Sample 2 shows a sharp edge, while in sample 3 an intermediate step with a width of approximately 200 μm can be discovered. Undissolved Cu clusters with a size of up to 20 μm are visible in both samples, which is also the maximum size of the base material Cu powder. The concentration of undissolved Cu particles in sample 2 is significantly lower, than in sample 3. The undissolved particles had a similar average diameter of 10.4 μm for sample 2 and 11.3 μm for sample 3, but the number of particles is up to twice as high for sample 3.

The sharp edge as well as the intermediate step in Cu concentration in the samples indicate complicated mechanical but laminar movement along the processing direction.

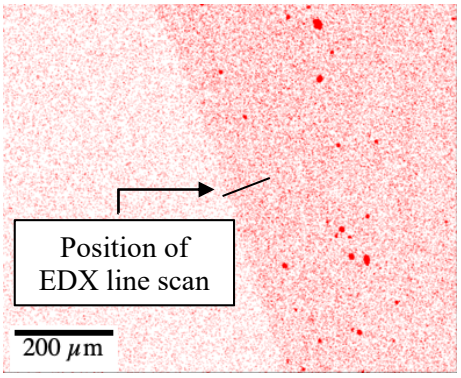

Figure 3. EDX mapping of the Cu concentration in sample 2 at the edge of the mechanically alloyed region. The position of the EDX line scan from Figure 5 is marked.

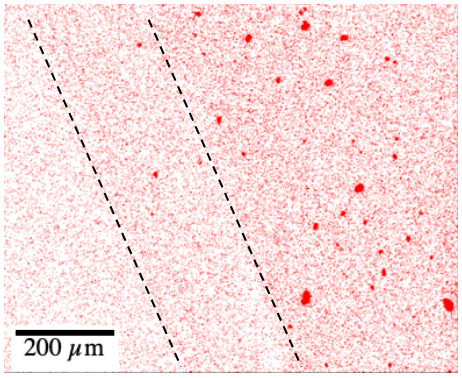

Figure 4. EDX mapping of the Cu concentration in sample 3 at the same position as in Figure 3.

To quantify the dissolved Cu content, an EDX line scan was carried out across the border region of sample 2. Its position is marked in Figure 3 and its result shown in Figure 5. The width of the region where the Cu concentration drops to 0 amounts to approximately 6 μm. Inside the mechanically alloyed region, the Cu concentration varies significantly between 0.2 and 0.34 *at%* along the measured line. More EDX spectra inside the stir zone were evaluated, which showed up to 0.73 *at%* for sample 2 and up to 0.56 *at%* for sample 3. This, together with the lower concentration of undissolved particles in sample 2 in comparison to sample 3 points out, that the higher rotation speed of 2250 *RPM* is more effective, then the 1500 *RPM* of sample 3, even though only two passes instead of four were executed. The strongly varying concentration and the sharp edge to the unalloyed region again suggest a complex laminar flow during dissolution. The strong concentration gradient accompanied by the changed material properties is furthermore interesting and could be exploited systematically.

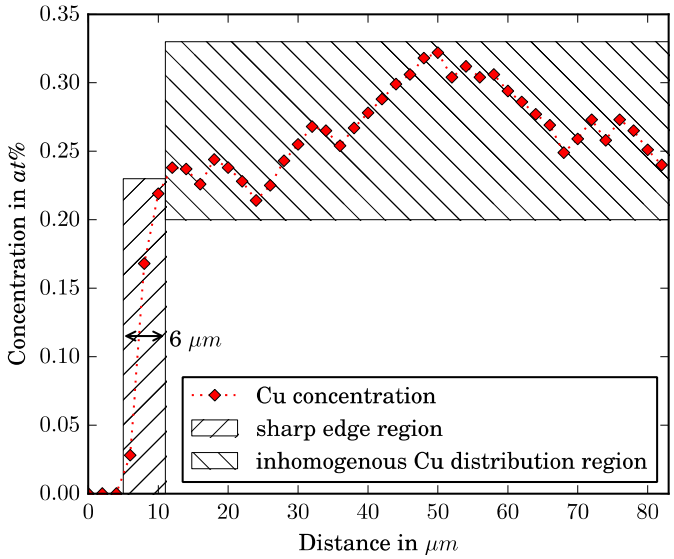

Figure 5. EDX line scan of Cu concentration of sample 2 at the position marked in Figure 2. The strongly fluctuation concentration profile inside the mechanically alloyed region as well as the clearly defined sharp edge is marked.

Sample 2 was subjected to high resolution transmission electron microscopy and showed intermetallic Θ'' precursor phases to the intentionally produced Θ' phase during age hardening of Al-Cu alloys. An image of one of these precipitations is shown in Figure 6. The formation of these phases at the elevated process temperature of approximately 400 *°C* inside the weld nugget (estimated from the temperature data measured by thermocouples) together with solid solution hardening are the reasons for the extreme hardness increase shown in Figure 7.

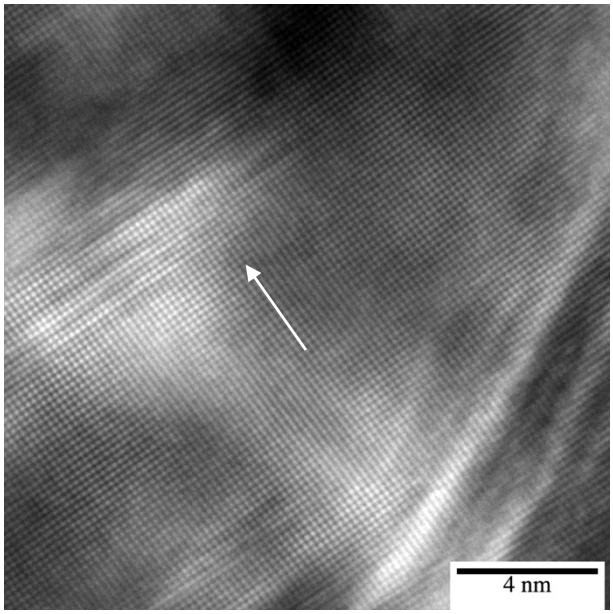

Figure 6. Θ'' phase formed during FSP visible via HRTEM and marked by arrow.

3.2. Mechanical properties

The findings of section 3.1 were believed to have strong impact on the mechanical properties of the mechanically alloyed and FSPed samples. Therefore, hardness mappings were recorded with 500 *mN* indentation force and 300 *µm* spacing between the indents and are shown in Figure 7. Sample 1 (Figure 7 (a)) shows no particle dissolution and a slight increase in hardness only around the particles, which did not get distributed effectively during FSP. Sample 2 (Figure 7 (b)) shows significant and reasonably homogenous hardening throughout the mechanically alloyed region up to values of 56 *HV*. Sample 3 (Figure 7 (c)) shows lower peak hardness values than sample 2 and the mechanically alloyed region has a more trapezoid shape.

The increased hardness values exactly match the contrast given by the Cu in the light microscopy images. Reasons for this enormous increase are solid solution hardening, formation of intermetallic precursor phases, as well as the unique microstructure with an average grain size of approximately 5 *µm* in the mechanically alloyed region (for all three samples).

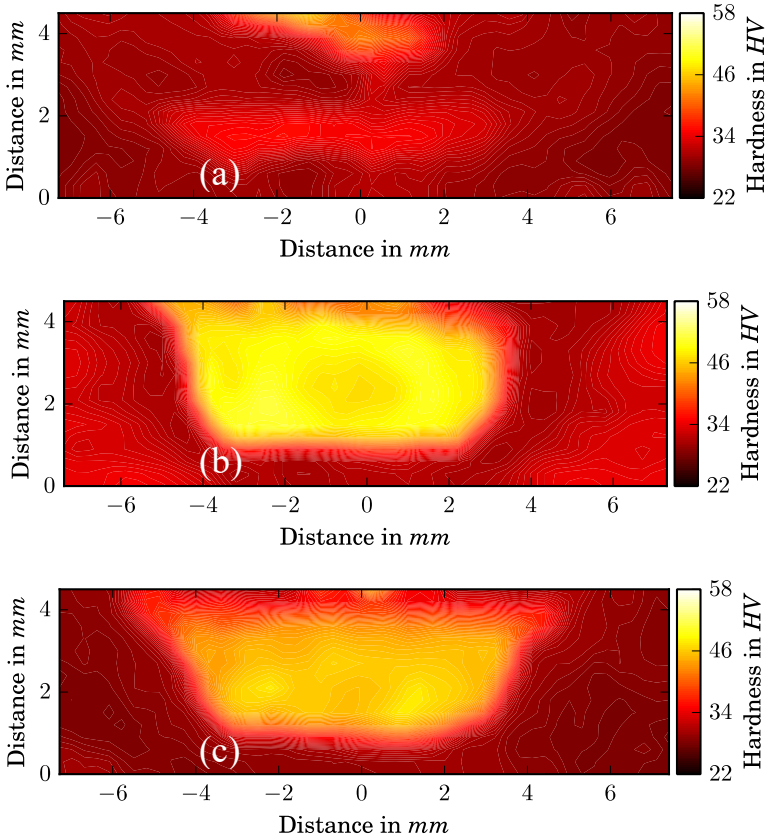

Figure 7. Hardness mappings recorded with a Berkovich indenter, 500 *mN* indentation force and 300 *µm* spacing between the indents. Sample 1 (a), sample 2 (b) and sample 3 (c)

4. Temperature measurements and modelling

To understand the different behaviour regarding the mechanically assisted dissolution depending on rotation speed and pass number, temperature measurements shown in Figure 8 were taken into account. The process temperature in direct proximity of the probe deviates from the measured one by up to 100 °*C*, which was proven in literature by measurements inside the probe [20]. Nevertheless, the relation between the temperature data of sample 2 and 3 can be evaluated to get insights into the reasons for the different outcome after FSP.

Beyond that, the diffusion length $\boldsymbol{d}$ depending on time $\boldsymbol{t}$ was incrementally calculated by Equation 1, assuming, that the Diffusion is thermally activated:

$$\boldsymbol{d(t)} = \int_0^{\boldsymbol{t}} \sqrt{\boldsymbol{t}\, \boldsymbol{D_0}\, e^{-\frac{\boldsymbol{Q}}{\boldsymbol{k_B T(t)}}}}\, \boldsymbol{dt} \tag{1}$$

With $\boldsymbol{T}$ being the temperature, which changes with time $\boldsymbol{t}$, $\boldsymbol{D_0}$ is the prefactor of diffusion, $\boldsymbol{Q}$ is the activation energy and $\boldsymbol{k_B}$ is the Boltzmann constant. Both $\boldsymbol{D_0}$ and $\boldsymbol{Q}$ where taken from [20]. The result for sample 2 and 3 is also plotted in Figure 8. Because sample 1 was produced with the same process parameters as sample 3 and thus yielded almost identical results, it was not taken into account.

It is obvious, that the reachable diffusion length of up to 100 *nm* does not contribute effectively to the distribution of Cu in the stir zone. While thermally activated, the diffusion is only occurring during

the tens of seconds when the temperature reaches its peak values during to the passage of the probe. Although this is sufficient to bring a small amount of Cu into solid solution.

With the temperatures of sample 2 and 3 being very similar and also constant across all passes (pass 4 of sample 3 was not recorded, due to software failure), no explanation is obvious. Even the noticeable higher rotation speed, with which sample 2 was produced, does not seem to have significant influence on the temperature.

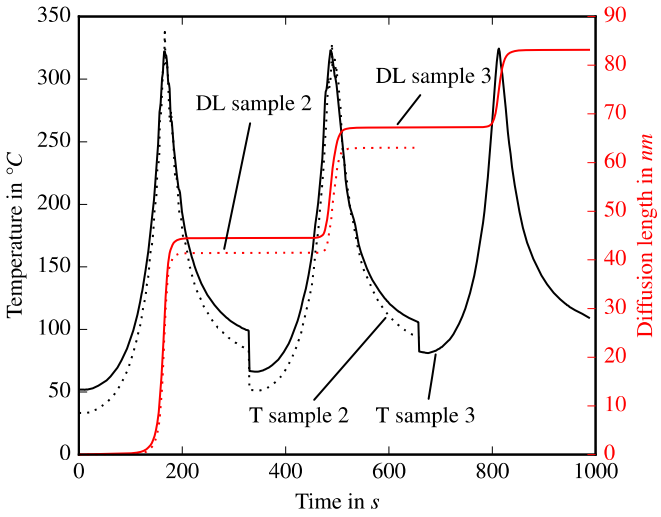

Figure 8. Attainable diffusion length in sample 2 and 3 over process time in pass 1 and 2 (sample 2) and passes 1, 2 and 3 (sample 3).

Comparing sample 1 and 3, there has to be a starting point of the Cu dissolution reaction even at constant rotation speed, just by increasing the pass number. This starting point is therefore assumed to be caused by a chain reaction, where enough Cu dissolved to harden the material, which in return leads to an increase of necessary deformation energy at constant rotation rate to dissolve more Cu. On the atomic length scale the effect could be caused by a change of dislocation movement. Once the coarse particles are parted by shear forces to a size at which it is energetically favorable to cut a particle instead of bypassing it, this chain reaction of mechanical dissolution can begin. Why this process does not have any effect on the temperature and why some of the Cu particles after the process still have their initial size is part of ongoing investigation.

5. Conclusions

- An effective mechanical alloying process starts with >1500 *RPM* and >2 passes at 50 *mm/min* feed rate for Cu in AA1050, but not all copper particles can be dissolved completely.
- Cu rich aluminium is apparently distributed in complex laminar and stable motion along the processing direction, which leads to significant variation in Cu content in stir zone.
- An extreme hardening effect is accomplished by solid solution hardening, the formation of intermetallic phases and the microstructure characteristic for FSP.
- Temperature measurements give no explanation for a starting point of the dissolution process.
- Complex interplay of interdiffusion at the particle matrix interface with subsequent hardening is suggested, which leads to chain reaction after the starting point of dissolution.
- Further investigations will include temperature measurements inside the probe and a raise of the Cu content to test, if a surpassing of the maximum solution limit is possible.

Acknowledgements

The research project HA 1549/6-1 is funded by the German Research Foundation (DFG). The authors would like to thank for the funding and the support. Also, David Stein and Florian Fleischmann shall be thanked for the support by practical help and fruitful discussions.

References

[1] Ogino Y, Yamasaki T, Murayama S and Sakai R 1990 Non-equilibrium phases formed by mechanical alloying of Cr · Cu alloys *J. Non. Cryst. Solids* **117**–**118** 737–40
[2] Gaffet E, Louison C, Harmelin M and Faudot F 1991 Metastable phase transformations induced by ball-milling in the Cu · W system *Mater. Sci. Eng. A* **134** 1380–4
[3] Gente C, Oehring M and Bormann R 1993 Formation of thermodynamically unstable solid solutions in the Cu-Co system by mechanical alloying *Phys. Rev. B* **48** 13244–52
[4] Gonzalez G, Sagarzazu A, Bonyuet D, D'Angelo L and Villalba R 2009 Solid state amorphisation in binary systems prepared by mechanical alloying *J. Alloys Compd.* **483** 289–97
[5] Karoline B, Kormout S, Pippan R and Bachmaier A 2016 Deformation-Induced Supersaturation in Immiscible Material Systems during High-Pressure Torsion ** 1–19
[6] Bachmaier A, Schmauch J, Aboulfadl H, Verch A and Motz C 2016 On the process of co-deformation and phase dissolution in a hard-soft immiscible Cu-Co alloy system during high-pressure torsion deformation *Acta Mater.* **115** 333–46
[7] Min G, Lee J-M, Kang S-B and Kim H-W 2006 Evolution of microstructure for multilayered Al/Ni composites by accumulative roll bonding process *Mater. Lett.* **60** 3255–9
[8] Rahmatabadi D, Mohammadi B, Hashemi R and Shojaee T 2018 An Experimental Study of Fracture Toughness for Nano/Ultrafine Grained Al5052/Cu Multilayered Composite Processed by Accumulative Roll Bonding *J. Manuf. Sci. Eng.* **140** 101001–11
[9] Hsieh C C, Shi M S and Wu W 2012 Growth of intermetallic phases in Al/Cu composites at various annealing temperatures during the ARB process *Met. Mater. Int.* **18** 1–6
[10] Zens A, Gnedel M, Zaeh M F and Haider F 2018 The effect of additive geometry on the integration of secondary elements during Friction Stir Processing *IOP Conf. Ser. Mater. Sci. Eng.* **373**
[11] Xu W F, Liu J H and Chen D L 2011 Material flow and core/multi-shell structures in a friction stir welded aluminum alloy with embedded copper markers *J. Alloys Compd.* **509** 8449–54
[12] Khorrami M S, Samadi S, Janghorban Z and Movahedi M 2015 In-situ aluminum matrix composite produced by friction stir processing using FE particles *Mater. Sci. Eng. A* **641** 380–90
[13] Lee I S, Kao P W and Ho N J 2008 Microstructure and mechanical properties of Al--Fe in situ nanocomposite produced by friction stir processing *Intermetallics* **16** 1104–8
[14] Hassan K A A, Norman A F, Price D A and Prangnell P B 2003 Stability of nugget zone grain structures in high strength Al-alloy friction stir welds during solution treatment *Acta Mater.* **51** 1923–36
[15] Zohoor M, Besharati Givi M K and Salami P 2012 Effect of processing parameters on fabrication of Al-Mg/Cu composites via friction stir processing *Mater. Des.* **39** 358–65
[16] Abnar B, Kazeminezhad M and Kokabi A H 2014 The Effect of Cu Powder During Friction Stir Welding on Microstructure and Mechanical Properties of AA3003-H18 *Metall. Mater. Trans. A* **45** 3882–91
[17] Hsu C J, Kao P W and Ho N J 2007 Intermetallic-reinforced aluminum matrix composites produced in situ by friction stir processing *Mater. Lett.* **61** 1315–8
[18] Hsu C J, Kao P W and Ho N J 2005 Ultrafine-grained Al--Al 2 Cu composite produced in situ by friction stir processing *Scr. Mater.* **53** 341–5
[19] Karthik G M, Ram G D J and Kottada R S 2017 Friction stir selective alloying *Mater. Sci. Eng. A* **684** 186–90
[20] Marstatt R, Krutzlinger M, Luderschmid J, Constanzi G, Mueller J F J, Haider F and Zaeh M F 2018 Intermetallic layers in temperature controlled Friction Stir Welding of dissimilar Al-Cu-joints *IOP Conf. Ser. Mater. Sci. Eng.* **373**